Global Analysis of Fluorescence Lifetime Imaging Microscopy Data

Peter J. Verveer, Anthony Squire, and Philippe I. H. Bastiaens
Cell Biophysics Laboratory, Imperial Cancer Research Fund, London WC2A 3PX, England

ABSTRACT Global analysis techniques are described for frequency domain fluorescence lifetime imaging microscopy (FLIM) data. These algorithms exploit the prior knowledge that only a limited number of fluorescent molecule species whose lifetimes do not vary spatially are present in the sample. Two approaches to implementing the lifetime invariance constraint are described. In the lifetime invariant fit method, each image in the lifetime image sequence is spatially averaged to obtain an improved signal-to-noise ratio. The lifetime estimations from these averaged data are used to recover the fractional contribution to the steady-state fluorescence on a pixel-by-pixel basis for each species. The second, superior, approach uses a global analysis technique that simultaneously fits the fractional contributions in all pixels and the spatially invariant lifetimes. In frequency domain FLIM the maximum number of lifetimes that can be fit with the global analysis method is twice the number of lifetimes that can be fit with conventional approaches. As a result, it is possible to discern two lifetimes with a single-frequency FLIM setup. The algorithms were tested on simulated data and then applied to separate the cellular distributions of coexpressed green fluorescent proteins in living cells.

INTRODUCTION

Fluorescence lifetime imaging microscopy (FLIM) allows the lifetimes of one or more fluorophores to be spatially resolved and can be used to provide information about the state of the fluorescent species and their immediate molecular environment. The fluorescence lifetime is sensitive to environmental conditions such as pH, and excited state reactions such as fluorescence resonance energy transfer (FRET) or collisional quenching, properties that have been exploited for resolving physiological parameters in the cell (Lakowicz et al., 1992, 1994; Gadella et al., 1993, 1999; Gadella and Jovin, 1995; Sanders et al., 1995; Szmancinski and Lakowicz, 1995; Bastiaens and Jovin, 1996; French et al., 1997; Bastiaens and Squire, 1999; Ng et al., 1999; Pepperkok et al., 1999). Fluorescence lifetime imaging in a wide-field or confocal microscope has been implemented, using time-domain and frequency-domain techniques (Lakowicz and Berndt, 1991; Buurman et al., 1992; Clegg et al., 1992; Gadella et al., 1994; Dong et al., 1995; Draaijer et al., 1995; So et al., 1995; Clegg and Schneider, 1996; Periasamy et al., 1996; Carlsson and Liljeborg, 1997; Schneider and Clegg, 1997; Sytsma et al., 1998; Squire and Bastiaens, 1999).

Until recently, fluorescence lifetime imaging has been limited to single lifetime estimates at each pixel of the sample image. However, in many cases a mixture of different molecular species or molecules in different biochemical states is present in each resolvable image element of the sample. As a result, the time-resolved response is a complex decay that is not described accurately by a single exponential. In such cases, a single lifetime estimation is only a semiquantitative measurement of the decay kinetics of the sample. Instead, the lifetimes and populations of each species should be resolved. For time domain measurements, this can be achieved by sampling the response to a light pulse and fitting a multiexponential function to the measurements. This approach was implemented in a microscope by Scully et al. (1996, 1997). In the frequency domain, the phase shifts and modulations must be recorded at multiple frequencies and the parameters of a multiexponential decay can then be derived using a nonlinear analysis algorithm (Gratton et al., 1984; Lakowicz et al., 1984). The latter technique was recently implemented by us in a microscope; we call this multiple-frequency fluorescence lifetime imaging microscopy (mfFLIM) (Squire et al., 1999). The mfFLIM technique opens the possibility of resolving a complex decay function and determining the lifetimes and populations of a number of species in each pixel. The signal-to-noise ratio of the data, however, is critical for obtaining a reliable result. Improving the signal-to-noise ratio is especially difficult for data acquired with fluorescence microscopy, because the exposure time is limited by factors such as photobleaching and, in the case of living cells, imaging speed. Similar limitations arise with the use of time domain techniques.

In this paper these problems are solved by applying a global analysis method to frequency domain FLIM image sequences in a fashion similar to techniques used for the analysis of fluorescence measurements in cuvettes (Knutson et al., 1983; Beechem et al., 1983, 1985; Beechem and Brand, 1986; Beechem, 1992; Gratton et al., 1984; Lakowicz et al., 1984). There, the results of multiple experiments are analyzed simultaneously, assuming that some of the parameters are identical for each experiment, while the remaining parameters may differ per experiment. The classical example is the resolution of a mixture of two fluores-

Received for publication 29 October 1999 and in final form 29 December 1999.

Address reprint requests to Dr. Philippe I. H. Bastiaens, Imperial Cancer Research Fund, Cell Biophysics Laboratory, 44 Lincoln's Inn Fields, London WC2A 3PX, England. Tel.: 44-171-269-3082; Fax: 44-171-269-3094; E-mail: p.bastiaens@icrf.icnet.uk.

0006-3495/00/04/2127/11 $2.00

cent species by lifetimes. The results of lifetime measurements are analyzed in terms of a biexponential model, resulting in the lifetimes and the fractional contributions to the steady-state fluorescence. This experiment can be repeated at different wavelengths, yielding data sets with different fractions, but the same lifetime values. It can be shown that simultaneous analysis of all data sets, using the knowledge that the lifetimes are invariant, yields vastly superior results compared to separate analysis of each set. The same lifetime invariance principle can be applied to the analysis of fluorescence lifetime images. Assuming that there is a given number of molecular species with different lifetimes, it is reasonable to assume that these lifetimes do not vary spatially. Thus, instead of analyzing each pixel separately, we analyze all pixels simultaneously, yielding images of the populations of each molecular species and the discrete lifetime values. In this paper we show that this approach leads to a dramatic improvement in the accuracy and precision of FLIM data analysis. In addition, we show that global analysis allows two lifetimes to be resolved by the use of a single-frequency measurement, which is fundamentally impossible by conventional data analysis techniques. We test the proposed analysis techniques on simulated data and use them to separate the fluorescence distributions of coexpressed green fluorescent proteins in living cells.

THEORY

Fluorescence lifetime measurements in the frequency domain

The theory of fluorescence lifetime measurements in the frequency domain has been described extensively (Clegg et al., 1992; Gratton and Limkeman, 1983; Gratton et al., 1984; Lakowicz et al., 1984; Clegg and Schneider, 1996; Gadella et al., 1994; Squire and Bastiaens, 1999). Here we repeat the most important results. The fluorescence response $R(t)$ of a sample to impulse excitation is a sum of Q exponential decays:

$$R(t) = \sum_{q=1}^{Q} \frac{\alpha_q}{\tau_q} \exp\left(-\frac{t}{\tau_q}\right), \tag{1}$$

where α_q and τ_q are the fractional contributions to the steady-state fluorescence and the lifetime from the qth emitting species, respectively. From the fractional contributions the relative populations a_q of each species can be found by dividing by the quantum yield of the fluorophore, corrected for the instrument response, and renormalizing the sum of the populations to one. If the spectra of all species are the same, this is equivalent to dividing by the lifetimes and renormalizing. Multiplying the populations a_q by the steady-state fluorescence yields the concentration of each species up to a constant multiplier.

In the frequency domain approach to FLIM the sample is illuminated by a periodically modulated excitation field that can be represented by a Fourier series:

$$E(t) = E_0 + \sum_{n=1}^{N} E_n \cos(n\omega t + \phi_{E,n}), \tag{2}$$

where ω is the fundamental circular frequency of the periodic excitation signal, N is the number of harmonics that are present, E_0 is the average intensity, and E_n and $\phi_{E,n}$ are the modulation and the phase of the nth harmonic. The fluorescence emitted by the sample is proportional to the convolution of the excitation light $E(t)$ with the response function $R(t)$:

$$F(t) \propto \int_{-\infty}^{t} E(u)R(t-u)\mathrm{d}u$$

$$= E_0 + \sum_{n=1}^{N} E_n M_n \cos(n\omega t + \phi_{E,n} - \Delta\phi_n), \tag{3}$$

where the phase shift $\Delta\phi_n$ and modulation M_n are given by

$$\Delta\phi_n = \arctan(A_n/B_n), \tag{4a}$$

$$M_n = (A_n^2 + B_n^2)^{1/2}, \tag{4b}$$

and

$$A_n = \sum_{q=1}^{Q} \frac{\alpha_q n\omega\tau_q}{1 + (n\omega\tau_q)^2}, \tag{5a}$$

$$B_n = \sum_{q=1}^{Q} \frac{\alpha_q}{1 + (n\omega\tau_q)^2}. \tag{5b}$$

To determine the fractions α_q and lifetimes τ_q, the modulations M_n and phase shifts $\Delta\phi_n$ must be measured for a number of frequencies and fitted to Eqs. 4 and 5.

To measure the modulations M_n and phase shifts $\Delta\phi_n$ in a microscope, heterodyne or homodyne phase detection techniques can be employed, using high-speed image intensifier devices (Gadella et al., 1993; Kume et al., 1988). These devices convert an image on the photocathode surface into electrons across the faces of a multichannel plate (MCP). These are then converted back to photons after they hit a photoluminescence surface. A repetitive high-frequency voltage modulation across either the MCP or the photocathode results in high-frequency modulation of the gain of the device. This makes it possible to modulate the detected fluorescence image at a frequency that is close (heterodyne detection) or equal (homodyne detection) to that of the excitation light. The resulting image only contains the low-frequency components of the modulated image, because high frequencies are filtered out by the slow

response of the photoluminescence surface at the output of the intensifier.

The time-dependent gain of the modulated intensifier can be represented by a Fourier series:

$$G(t) = G_0 + \sum_{m=1}^{M} G_m \cos(m\omega' t + \phi_{G,m} - mk\Delta\psi), \quad (6)$$

where ω' is the fundamental circular frequency of the gain modulation. G_0 is the average gain, and G_m and $\phi_{G,m}$ are the amplitude and the phase of the mth harmonic. The phase of $G(t)$ can be controlled by adjusting $k\Delta\psi$). The resulting image is given by the low-frequency components of the result of multiplying Eq. 3 by Eq. 6. For homodyne detection the output image can be written as

$$D(k) = D_0\left(1 + \sum_{n=1}^{N} M_{R,n}M_n \cos(nk\Delta\psi - \Delta\phi_n - \phi_{R,n})\right), \quad (7)$$

where $M_{R,n} = E_nG_n/2E_0G_0$ is the reference modulation, and $\phi_{R,n} = \phi_{G,n} - \phi_{E,n}$ is the reference phase, which must be obtained from an independent measurement on a sample with a known lifetime. D_0 is the average intensity, which depends on factors such as photon detection efficiency, intensity of excitation, and fluorophore quantum yield. D_0 is proportional to the steady-state fluorescence from the sample. The signal $D(k)$ is time-independent and can be phase-sampled at discrete phases $k\Delta\psi$. Equation 7 can be transformed to a linear equation (Gadella et al., 1994; Squire and Bastiaens, 1999), the parameters of which can be estimated using a Fourier transform, or singular value decomposition (Press et al., 1992), where the latter allows estimation of errors for M_n and $\Delta\phi_n$ (Squire and Bastiaens, 1999).

Given the modulations M_n and phase shifts $\Delta\phi_n$, it is possible to compute the fractions α_q and lifetimes τ_q, using Eqs. 4 and 5. For the case of only a single lifetime ($Q = 1$, $\alpha_Q = 1$), the lifetime value can be calculated directly from either modulation or phase shift:

$$\tau_{\Delta\phi,n} = \tan(\Delta\phi_n)/n\omega, \quad (8a)$$

$$\tau_{M,n} = (1/M_n^2 - 1)^{1/2}/n\omega. \quad (8b)$$

If the assumption of a monoexponential decay model is correct, then $\tau_{\Delta\phi,n} = \tau_{M,n}$, and the values are independent of the frequency $n\omega$. Differences in the lifetime estimations from phase shift and modulations indicate that the decay kinetics of the sample are more complex.

In the case of a multiexponential decay model, a nonlinear fit to Eqs. 4 and 5 can be used to obtain the populations and lifetimes (Gratton et al., 1984; Lakowicz et al., 1984; Squire et al., 1999).

Global analysis of phase-modulation image data

The analysis that was outlined above can be applied on a pixel-by-pixel basis to a phase-dependent sequence of FLIM images. For microscope samples, the need to minimize photobleaching and acquisition time limits the number of frequencies at which measurements are taken. This can lead to a signal-to-noise ratio that is low, leading to inaccurate results. A solution to this problem is to reduce the number of variables that have to be estimated by employing prior knowledge about the sample.

First we note that the α_q are fractional contributions to the steady-state fluorescence and that their sum equals one. Therefore, we eliminate one variable at each pixel by substituting $\alpha_Q = 1 - \Sigma_{q=1}^{Q-1}\,\alpha_q$. This allows us to rewrite Eq. 5:

$$A_n = \frac{n\omega\tau_Q}{1 + (n\omega\tau_Q)^2} + \sum_{q=1}^{Q-1}\left(\frac{n\omega\tau_q}{1 + (n\omega\tau_q)^2} - \frac{n\omega\tau_Q}{1 + (n\omega\tau_Q)^2}\right)\alpha_q, \quad (9a)$$

$$B_n = \frac{1}{1 + (n\omega\tau_Q)^2} + \sum_{q=1}^{Q-1}\left(\frac{1}{1 + (n\omega\tau_q)^2} - \frac{1}{1 + (n\omega\tau_Q)^2}\right)\alpha_q. \quad (9b)$$

These equations are linear in α_q, and if the lifetime values are known, the populations can be found by a linear least-squares method, for instance, a singular value decomposition.

An important form of prior knowledge is that in many applications the lifetimes are spatially invariant. Each pixel in the image represents a mixture of different fluorophores or molecules in different biochemical states. This gives rise to a multiexponential decay whose lifetimes do not vary spatially. One simple approach to making use of that knowledge was implemented by us previously and termed the "lifetime invariant fit" (Squire et al., 1999). In this approach, the intensities of each image in the FLIM sequence are averaged to a single value. This gives a phase-dependent data series with an increased signal-to-noise ratio at the expense of spatial information. The lifetimes of each fluorescent species can then be obtained by estimating the phase shifts and modulations from this averaged series, followed by a nonlinear analysis, as described in the previous section. The fractional contributions in each pixel can then be recovered by substituting these lifetime values back into Eq. 9.

A second approach utilizes global analysis (Knutson et al., 1983; Beechem et al., 1983, 1985; Beechem and Brand, 1986; Beechem, 1992; Gratton et al., 1984; Lakowicz et al., 1984), where all pixels are analyzed simultaneously and the lifetimes are constrained to be the same in each pixel. This is accomplished by nonlinear minimization of the following χ^2 measure, summing over N harmonic frequencies, and M

pixels in the image:

$$\chi^2(\alpha_{q,m}, \tau_q) = \sum_{m=1}^{M} \sum_{n=1}^{N} \left[\left(\frac{\hat{A}_{n,m} - A_{n,m}(\alpha_{q,m}, \tau_q)}{\sigma(A_{n,m})} \right)^2 + \left(\frac{\hat{B}_{n,m} - B_{n,m}(\alpha_{q,m}, \tau_q)}{\sigma(B_{n,m})} \right)^2 \right], \quad (10)$$

where $\hat{A}_{n,m}$ and $\hat{B}_{n,m}$ are calculated from the measured phase shift and modulation in the mth pixel for the nth frequency, using Eq. 4, and $\sigma(A_{n,m})$ and $\sigma(B_{n,m})$ are estimates of their standard deviation, calculated by error propagation from the errors in the phase shift and modulation. The expressions for $A_{n,m}(\alpha_{q,m}, \tau_q)$ and $B_{n,m}(\alpha_{q,m}, \tau_q)$ are given by Eq. 9, where the subscript m was added to indicate that the fractions differ at each pixel. The parameters that are varied to minimize this χ^2 measure are the Q lifetime values τ_q and the M sets of $Q - 1$ fractions $\alpha_{q,m}$. Minimization of Eq. 10 is a separable nonlinear least-squares problem that can be solved by dedicated algorithms (Golub and Pereyra, 1973). However, for a large number of variables the memory requirements for such algorithms are too high. For typical FLIM data, tens to hundreds of thousands of independent variables must be estimated, and we therefore used a truncated Newton algorithm (Schlick and Fogelson, 1992) to directly minimize Eq. 10. With this minimization algorithm, typical computation times are on the order of a few minutes on a Sun Ultra 60 workstation for a typical FLIM sequence, where each image has ~100,000 pixels. Note that for a global analysis, the $\hat{A}_{n,m}$ and $\hat{B}_{n,m}$ images are calculated in a manner identical to that of a conventional analysis, where lifetime estimates are calculated on a pixel-by-pixel basis, using Eq. 8.

The two approaches described for implementing the spatial invariance constraint are fundamentally different. The lifetime invariant fit improves the signal-to-noise ratio to get an accurate estimation of the lifetime values. With these values, an accurate estimation of the fractions can be made. In contrast, the global fit makes use of the spatial variation in fractions, information that is lost in lifetime invariant fit because of the averaging operation. This difference has important consequences for the number of lifetimes that can be estimated for a given number of frequencies. For a successful fit, the number of parameters to be estimated must be less than or equal to the number of independent measurements. In a conventional fit, Q lifetimes, with $Q - 1$ populations, must be estimated from the phase shifts and modulations for N frequencies. Thus the following inequality must hold:

$$2Q - 1 \leq 2N \Rightarrow Q \leq N. \quad (11)$$

It follows that the number of lifetimes that can be estimated is less than or equal to the number of frequencies measured. This still holds true for the lifetime invariant fit, which is essentially a conventional fit of spatially averaged data. In the case of a global fit Q lifetimes must be estimated along with $Q - 1$ fractions in each pixel, from N phase shifts and modulations in M pixels. The requirement for a successful fit then becomes

$$M(Q - 1) + Q \leq 2MN \Rightarrow Q \leq 2N \quad \text{if } M \geq Q. \quad (12)$$

Thus we find that with a global fit we can potentially fit twice the number of lifetimes compared to a conventional analysis. In mfFLIM, where the total sample exposure should be minimized, this is an advantage, because the Nyquist criterion requires that the number of phase images is larger than twice the number of frequencies. Another significant consequence of Eq. 12 is that in principle it is possible to resolve two lifetimes and their populations ($Q = 2$) with the single frequency excitation in a standard FLIM setup ($N = 1$).

RESULTS

Simulated data

The two different approaches for fitting FLIM data were tested on simulated data. A biexponential decay model was assumed, with a long lifetime of 2 ns, and a shorter lifetime, which, for different simulations, was either fixed or varied. An image of 64 × 64 pixels was generated with fractions for the short lifetime species according to the formula $\alpha_{1,m} = m/M$, where m was the number of the pixel, counting in a one-dimensional fashion from the upper left to the lower right corner of the image, and M was the number of pixels. The fractions for the longer lifetime were $\alpha_{2,m} = 1 - \alpha_{1,m}$. These fractions were the same in all simulations. Multiple-frequency data with a fundamental frequency of 80 MHz and four harmonics was generated using Eq. 7, with reference phases $\phi_{R,1} = 0$, $\phi_{R,2} = 0.1$, $\phi_{R,3} = 0.2$, $\phi_{R,4} = 0.3$, and reference modulations $M_{R,1} = 1$, $M_{R,2} = 0.8$, $M_{R,3} = 0.6$, $M_{R,4} = 0.4$. In addition, single-frequency FLIM data at 80 MHz were generated with $\phi_{R,1} = 1$. In both cases the number of phase sampling points was 32. Poisson noise was then added to the phase-dependent images, where the average intensity D_0 was varied to control the signal-to-noise ratio.

Fig. 1 shows the results of the different fit approaches for a simulated image, with the short lifetime equal to 1.5 ns and an average intensity over all phase images of $D_0 = 1000$ counts at each pixel. Shown are images of the original and recovered fractions along with the estimated lifetimes. The top row shows the results for the multiple-frequency data. Both the lifetime invariant fit and the global fit give accurate results; however, the conventional pixel-by-pixel fit fails completely. The bottom row shows the result for the single-frequency data. The global fit was capable of recov-

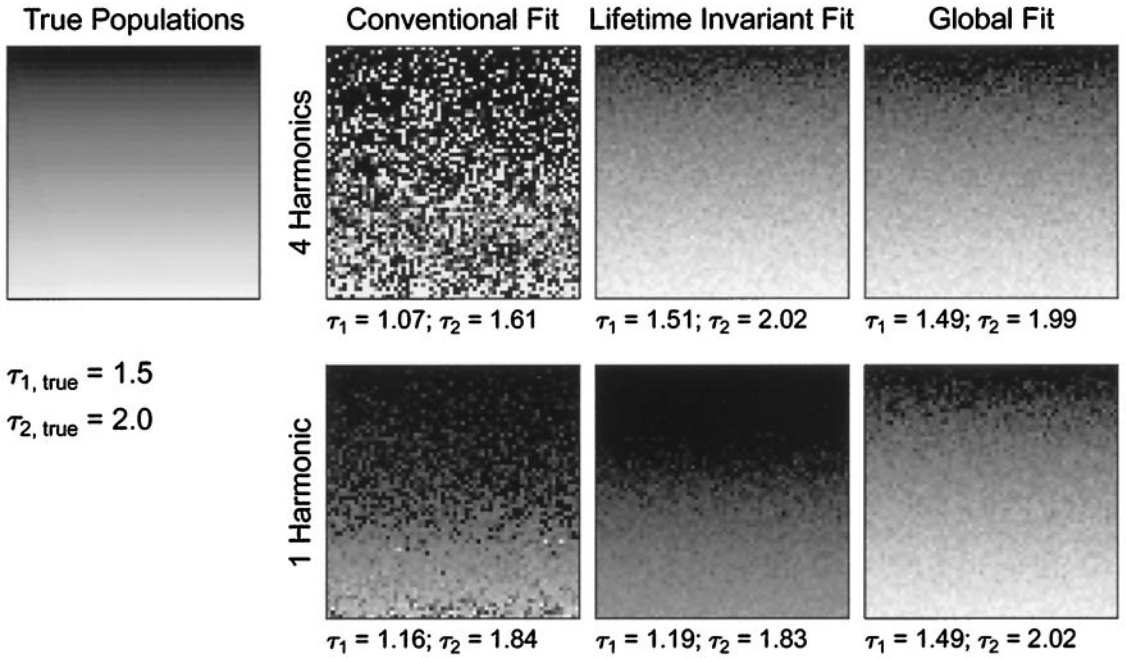

FIGURE 1 Images of fractions of the steady-state fluorescence associated with the short lifetimes species, from different fitting approaches to simulated FLIM data with four harmonics and with a single harmonic. Below each image the estimated lifetime values are given in nanoseconds. In the case of the conventional fit the average is shown for the pixels, where the lifetime values were between 0 ns and 2.5 ns. For display purposes fraction values below zero and above one were clipped, multiplied by 255, and the image was quantized to 8 bits. See text for further simulation parameters.

ering the lifetimes and fractions, whereas the conventional pixel-by-pixel and lifetime invariant fits fail to recover the correct values, as expected for an underdetermined fit.

Fig. 2 shows the estimated lifetime values as a function of the short lifetime value, where the long lifetime is fixed at 2 ns. The simulations were repeated 25 times with different realizations of a set amount of Poisson noise to compute average values and standard deviations. For the case of a conventional fit, the estimated values were the averages over the pixels, where the estimated value was between 0 ns and 2.5 ns. Clearly the conventional pixel-by-pixel fit performs very badly, except for large differences between the true lifetimes. The lifetime invariant fit performs much better as long as the true lifetime values are not too close. The global fit performs even better for lifetime values separated by as little as 0.2 ns. Fig. 3 shows the same results for data with a single harmonic. In this case the conventional fit and the lifetime invariant fit are not capable of estimating the correct values, whereas the global fit performs more or less as well as the global fit of the data with four harmonics. The results for the conventional and spatial invariant fits are not as bad as one might expect for these underdetermined fits and show a trend similar to that of the multifrequency results. Apparently, for this choice of lifetimes and frequency, the nonlinear least-squares minimization converges to a point that is not very far from the true values. However, the large standard deviations indicate that in general the results for the conventional and spatial invariant fits of single-frequency data cannot be expected to be correct.

To investigate the dependence on the signal-to-noise ratio of the data, simulations were performed, where the average intensity of the data was varied to control the amount of noise. Because the mean of the Poisson process is the intensity of the simulated phase image, an increased average of the phase-dependent data means an increase in detected photons and thus an increase in the signal-to-noise ratio. Fig. 4 shows the estimated lifetime values and standard deviations as a function of the average intensity for the different fit approaches using four harmonics. The true lifetime values were 1.5 ns and 2 ns. Average values and standard deviations were calculated from 25 repetitions of the simulation. In the case of the conventional fit the plotted lifetimes are the average of the pixels with estimated lifetime values between 0 ns and 2.5 ns. It can be seen that the conventional pixel-by-pixel fit fails. The global fit performs much better than the lifetime invariant fit, especially for low average intensity (low signal-to-noise ratio) values.

In all of these simulations the conventional pixel-by-pixel fit performs badly, indicating that for a typical FLIM measurement the signal-to-noise ratio is too low for an adequate pixel-by-pixel fit. For multiple-frequency data, the spatial invariant fit performs much better if the true lifetime values are well separated. The global fit is clearly superior to the two other methods and is the only approach that can be used

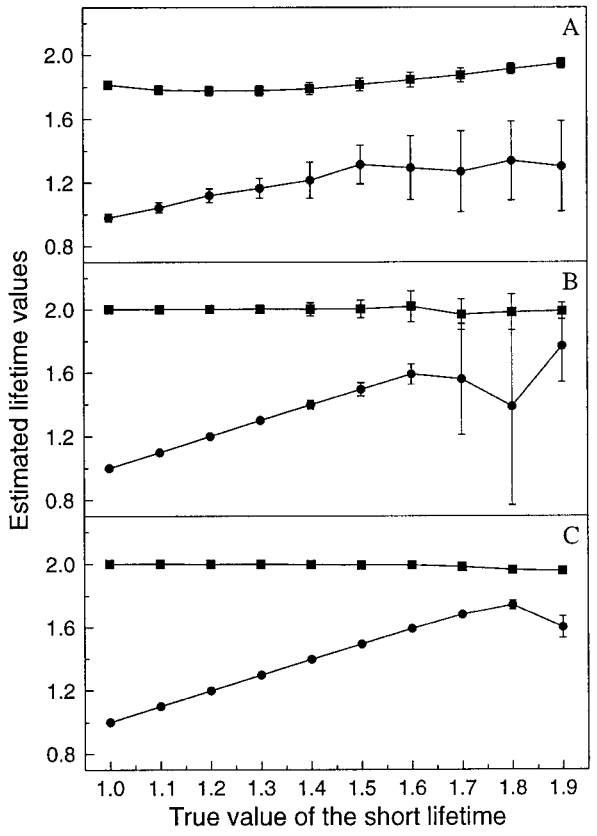

FIGURE 2 Estimated lifetime values as a function of the short lifetime value for the different fitting approaches on FLIM data with four harmonics. For the conventional fit the average of the pixels with estimated lifetimes between 0 ns and 2.5 ns was used. Shown are average estimated values and standard deviations from 25 data sets with different realizations of Poisson noise. If a point shows no error bars, the standard deviation was too small to be plotted. (*A*) Conventional fit; (*B*) lifetime invariant fit; (*C*) global fit.

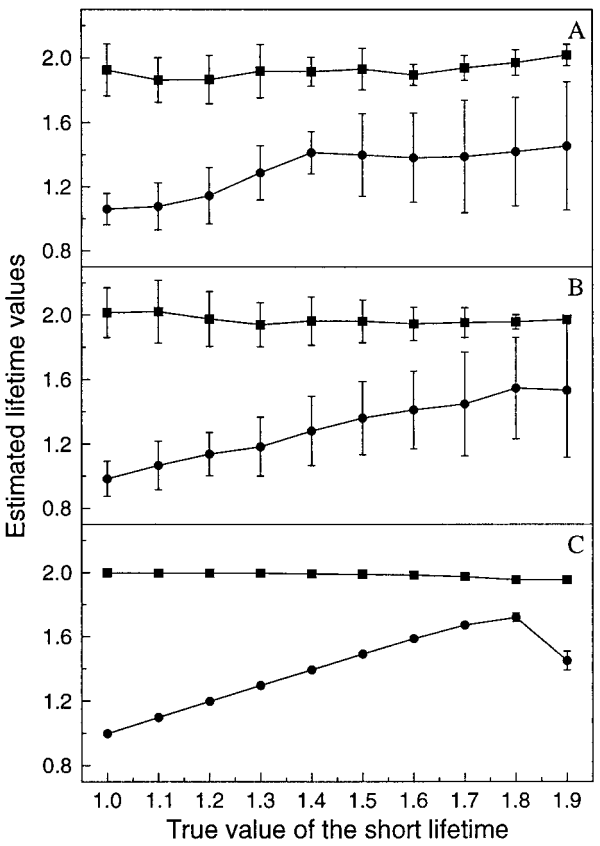

FIGURE 3 Estimated lifetime values as a function of the short lifetime value for the different fitting approaches on FLIM data with a single harmonic. For the conventional fit the average of the pixels with estimated lifetimes between 0 ns and 2.5 ns was used. Shown are average estimated values and standard deviations over 25 data sets with different realizations of Poisson noise. If a point shows no error bars, the standard deviation was too small to be plotted. (*A*) Conventional fit; (*B*) lifetime invariant fit; (*C*) global fit.

to accurately fit a two-component model to single-frequency data.

Experimental data

The global analysis algorithm was used to disentangle the cellular distributions of coexpressed green fluorescent proteins with different lifetimes in living cells. Vero cells were plated on Matek Petri dishes (Matek Corp.) in minimum essential medium supplemented with 5% fetal calf serum. These were microinjected in the nucleus with cDNA encoding plasmids for the yellow fluorescent protein (YFP5), which distributes evenly throughout the cytosol and nucleus, and a green fluorescent fusion protein (NLS-GFP5) that remains largely located in the nucleus (Pepperkok et al., 1999). The cells were washed and submerged in CO_2 independent medium (GibcoBRL) before they were measured at 37°C. The same procedure was used to coexpress a Golgi resident green fluorescent fusion protein (NA-GFP5) and YFP5 in Vero cells.

Phase-dependent images were collected using the mfFLIM setup that was described in detail by Squire et al. (1999). Excitation was with a 488-nm argon/krypton laser line. The fluorescence emission was detected through a filter block containing a dichroic beam-splitter 505LP in combination with either a High Q bandpass filter 515/10 BP for the Hela cells or with a 540/50 BP for the Vero cells (Delta Light and Optics). The sample was illuminated and the fluorescence collected with a Zeiss Plan Apochromat 100×/1.4 NA ph3 oil objective. The frequency of the fundamental harmonic was 39.175 MHz. A Fourier analysis of mfFLIM reference data from a reflecting sample showed that at least five significant harmonics were present, and therefore five harmonics were assumed for determining the modulations and phase shifts in the data. The first three harmonics had a modulation depth larger than 25%, and only these were used in the further global analysis of the

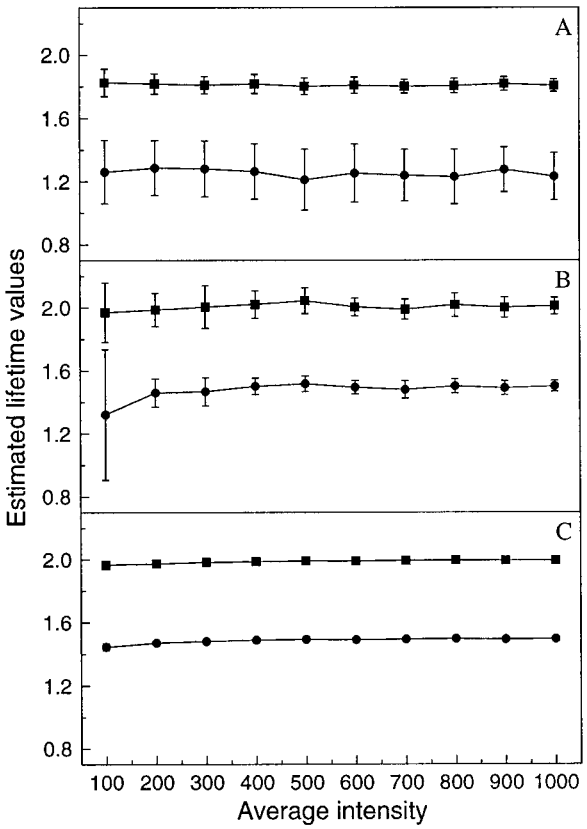

FIGURE 4 Estimated lifetime values as a function of the average intensity from an analysis of FLIM data with four harmonics. For the conventional fit the average of the pixels with estimated lifetimes between 0 ns and 2.5 ns was used. Shown are average estimated values and standard deviations over estimations from 25 data sets with different realizations of Poisson noise. If a point shows no error bars, the standard deviation was too small to be plotted. (*A*) Conventional fit; (*B*) lifetime invariant fit; (*C*) global fit.

data. For each sample 16 phase-dependent images at 22.5° phase steps with 200-ms exposure were collected. To compensate in first order for photobleaching, a second sequence of 16 images was collected by phase sampling backward, which were added to the first set (Gadella et al., 1994). For our data this first-order correction was sufficient for the relative short exposure times that were used. Before analysis, a background correction was applied to each phase-dependent image by subtracting the mean pixel value within a flat region outside the cell. A mask was then generated by thresholding the first image in the FLIM sequence. Only pixels within the mask were used in the global analysis. The mfFLIM data were also used to test the concepts of global analysis of single-frequency data. For each of the first three harmonics a single-frequency global analysis was performed, which is equivalent to global analysis of data acquired with a single-frequency FLIM instrument. In addition these three harmonics were used in a multiple-frequency global analysis of the data.

The lifetime values that are found for the different GFP variants by each analysis are given in Table 1. The value of ~3.6 ns that was found for YFP5 does not vary much for different frequencies, and the same value is recovered by single- and multiple-frequency analysis. This indicates that the decay kinetics of YFP5 are well described by a mono-exponential decay. In contrast, the values found for NLS-GFP5 and NA-GFP5 vary strongly with frequency. This indicates that the decay kinetics of these GFPs are complex. These observations are in agreement with previous measurements by Pepperkok et al. (1999) at a single frequency (80 MHz), where the lifetimes were calculated from phase shift and modulation, using Eq. 8. These results indicated that YFP5 is indeed homogeneous, with a lifetime of ~3.6 ns. The decays of NLS-GFP5 and NA-GFP5 were found to be heterogeneous, with estimations of 1.92 ns and 2.05 ns from the phase, and 2.25 ns and 2.40 ns from the modulation.

Single-frequency measurements are most sensitive at values of $\tau \approx 1/\omega$ and thus detect the fluorescence of short lifetime components more efficiently as the frequency increases. The estimated lifetime values of NLS-GFP5 and NA-GFP5 in Table 1 decrease with increasing frequency, indicating that the measurements become sensitive for a short component in the decay kinetics of these GFP variants. Thus, for higher modulation frequencies, the analysis is more strongly influenced by the choice of an incorrect two-component model, and consequently the estimated populations are more likely to be erroneous. The multiple-frequency analysis is also sensitive to such model errors, because it makes use of information obtained at multiple harmonics. By choosing a sufficiently low frequency in a single-frequency analysis, one can filter out short lifetime components to obtain an adequate fit of the long component. This approximation works well because the integrated fluorescence contribution from the short component can be neglected.

The fluorescence intensity from each species of molecule can be found by multiplying the steady-state fluorescence by the fractions obtained by global analysis. Fig. 5 gives the steady-state fluorescence intensity of the data with the calculated intensities of NLS-GFP5 and YFP5 for the single-frequency calculation at 39.175 MHz and for the multiple-

TABLE 1 Lifetime values of different GFP variants coexpressed in Vero and Hela cells obtained by global analysis of mfFLIM data

	Vero cells		Hela cells	
	$\tau_{\text{NLS-GFP5}}$ (ns)	τ_{YFP5} (ns)	$\tau_{\text{NA-GFP5 (ns)}}$	τ_{YFP5} (ns)
39.175 MHz	1.85	3.71	2.06	3.57
78.35 MHz	1.41	3.65	1.52	3.52
117.525 MHz	0.95	3.56	1.09	3.50
Multiple-frequency	1.18	3.61	1.38	3.56

Data are analyzed using the first three harmonics separately and using the first three harmonics simultaneously.

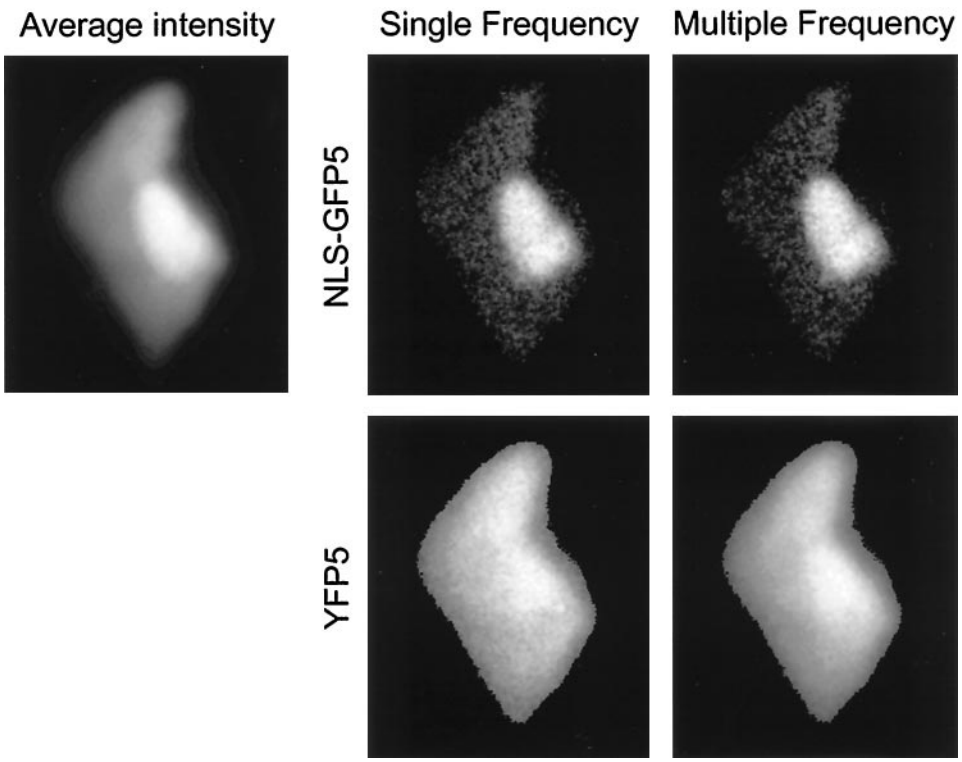

FIGURE 5 Global analysis of mf-FLIM data of coexpressed NLS-GFP5 and YFP5 in Vero cells. Shown are the average intensity (steady-state fluorescence) and the intensities of each species calculated by global analysis. The single-frequency analysis was calculated from the fundamental harmonic in the data. The multiple-frequency analysis was calculated from the first three harmonics in the data.

frequency analysis. The intensities of the NLS-GFP5 and YFP5 are disentangled effectively by the global analysis and show that the NLS-GFP5 is located mainly in the nucleus, while the YFP5 is distributed evenly throughout the cell as expected. Because of the heterogeneous nature of NLS-GFP5, the two-component model used by in the analysis is not correct, and the multifrequency analysis should be more sensitive to this model error than the single-frequency measurement at 39.175 MHz. Despite this, the intensity images from the two analysis approaches do not appear to differ.

Similar results can be seen in Fig. 6, where the intensities of NA-GFP5 and YFP5 are separated. The global analysis effectively separates the Golgi from the rest of the cell. In particular note the Golgi at the top of the image that is not clearly visible in the average intensity image because it is hidden by the high intensity of YFP5. YFP5 diffuses throughout the cytosol and nucleus, but it does not enter the Golgi. Thus the intensity of YFP5 should be lower in the Golgi, although it will not be zero, because of out-of-focus contributions from other parts of the cell. Fig. 7 focuses on the lower part of the images in Fig. 6. Fig. 7 *A* shows that in the single-frequency analysis at 39.175 MHz the intensity of YFP5 is indeed lower in the Golgi, while in the multiple-frequency analysis (Fig. 7 *B*) this is not the case. The difference is emphasized in Fig. 7 *C*, which shows the division of Fig. 7 *A* and Fig. 7 *B*. The lifetime value for NA-GFP5 found by the multifrequency analysis is a weighted average of the true lifetimes that does not characterize well the complex decay kinetics of the NA-GFP5 fluorescence. This model error propagates to the estimation of the fractional fluorescence of each species. In the single-frequency analysis at 39.175 MHz this model error appears to be much smaller. For comparison, the NA-GFP5 fluorescence is shown in Fig. 7 *D*, indicating that at 39.175 MHz the single-frequency analysis adequately disentangles the fluorescence distributions.

CONCLUSIONS

We have shown that the application of global analysis algorithms can significantly improve the accuracy and precision of lifetime and population estimations from FLIM and mfFLIM data. We employ the prior knowledge that each pixel contains a mixture of different fluorophores or fluorescently tagged molecules in different biochemical states, which gives rise to a multiexponential fluorescence decay, the lifetimes of which do not vary spatially. The parameters of interest are the lifetimes of each molecular species and the populations of all species in each pixel. Two approaches to making use of the spatial invariance of the lifetimes were implemented. The first approach averages the phase-dependent data spatially to increase the signal-to-noise ratio at the cost of lost spatial information. From these averaged data an accurate estimation of the lifetimes can be made. The estimated lifetimes from this lifetime invariant fit are used to recover the populations in each pixel. The second approach uses global analysis algorithms that analyze all pixels simultaneously, while constraining the lifetimes in all pixels to be equal.

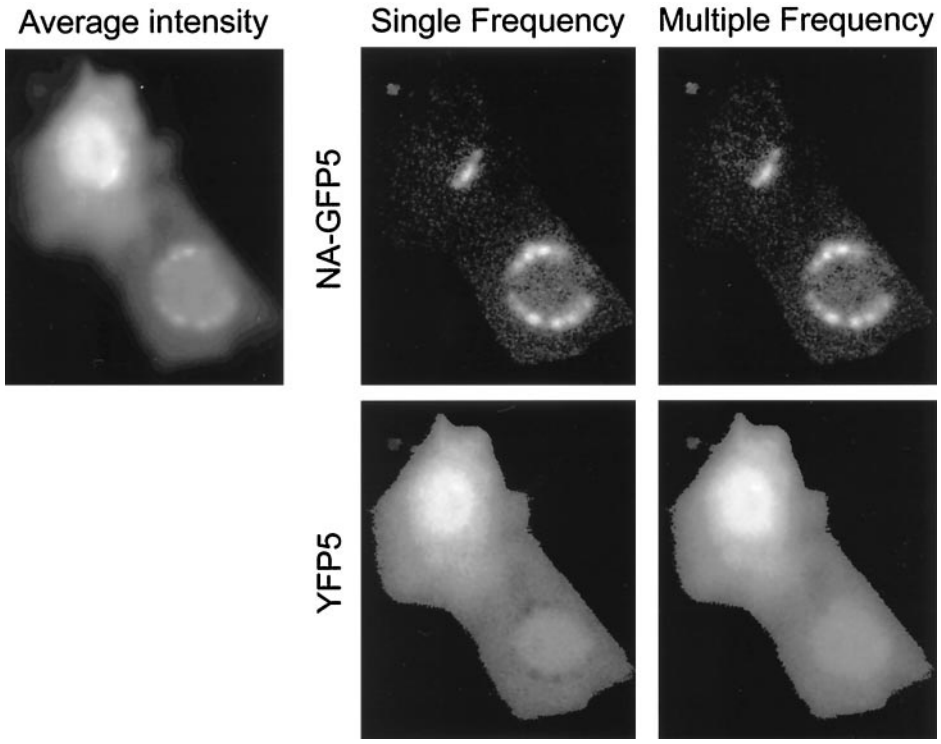

FIGURE 6 Global analysis of mf-FLIM data of coexpressed NA-GFP5 and YFP5 in Hela cells. Shown are the average intensity (steady-state fluorescence) and the intensities of each species calculated by global analysis. The single-frequency analysis was calculated from the fundamental harmonic in the data. The multiple-frequency analysis was calculated from the first three harmonics in the data.

It was shown that for a given number of harmonics the global fit is capable of fitting twice the number of lifetimes compared to a conventional pixel-by-pixel fit or a spatial invariant fit. This is an important property because applications in fluorescence microscopy often require that exposure times be minimized, which can be achieved by decreasing the number of frequencies. Another important consequence is that it becomes possible to resolve two lifetimes with a single-frequency FLIM setup. This is of importance because these types of lifetime microscopes are simpler to implement and more widespread than multiple-frequency setups.

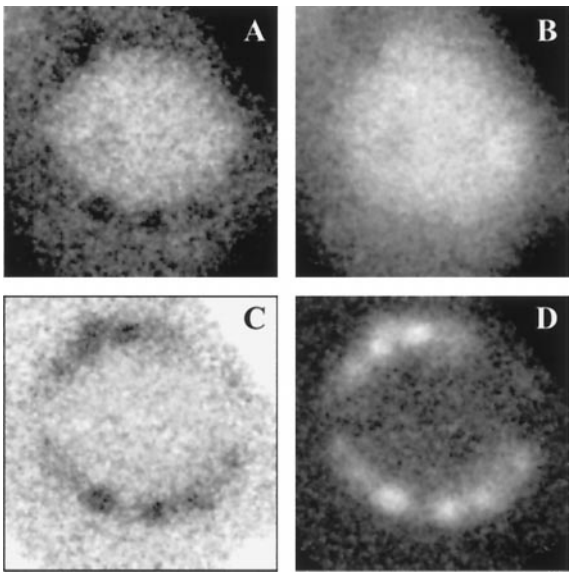

FIGURE 7 Comparison of the Golgi/nucleus area from Fig. 6. (*A*) Enlarged and contrast-stretched region from the single-frequency analysis of the YFP5 fluorescence. (*B*) The corresponding enlarged and contrast-stretched region from the multiple-frequency analysis of the YFP5 fluorescence. (*C*) Division of *A* and *B* to enhance the differences. (*D*) The corresponding enlarged and contrast-stretched region from the single-frequency analysis of the NA-GFP5 fluorescence.

Using simulations, it was found that both approaches are far superior to a conventional pixel-by-pixel fit. It was also found that the global analysis was superior to the lifetime invariant fit. This can be explained by the fact that the global analysis approach can make use of spatial information, whereas the spatial invariant fit just improves the estimation of the lifetimes by increasing the signal-to-noise ratio at the cost of that spatial information. The global analysis performs much better, particularly at low signal-to-noise ratios, which is important if the noise in the FLIM sequence is larger, for instance, in applications that require rapid imaging of living cells.

The global analysis algorithm was applied to disentangle the fluorescence intensities of coexpressed green fluorescent proteins in living cells. It was found that this is possible, even if the assumption that each fluorophore has mono-exponential decay kinetics is only an approximation. Short components in a complex decay can be filtered out in a single-frequency measurement by carefully choosing a modulation frequency where its contribution to the fluorescence is small. Adequate results can then be obtained if the

decay behaves effectively as a monoexponential with a lifetime approaching the long component of the complex decay. A multifrequency analysis also makes use of the information contained in the higher harmonics and is therefore sensitive to short components in a complex decay. As a result, the analysis of multifrequency measurements may be more sensitive to errors in the decay model that is assumed in the analysis. In the case where one or more fluorophores are present with a complex decay, it is appropriate to fit mfFLIM data with the correct multiexponential model to obtain more accurate results. However, fitting more than two components is a far more complex problem than fitting a two-component model (Gratton et al., 1984; Lakowicz et al., 1984). This problem might be solved by an algorithm that exploits the knowledge that a fluorophore has a multiexponential decay with fixed relative amplitudes. Resolution of fluorophores with complex decays and separation of more than two fluorophores continues to be a topic of research.

In this work, the global analysis technique was applied to FLIM in the frequency domain; however, we expect that similar gains can be achieved with systems that operate in the time domain. Another interesting application would be to photobleaching data (Jovin and Arndt-Jovin, 1989), which follow exponential decay kinetics with decay times that are inversely proportional to the lifetime of the fluorophore.

Fluorescence energy resonance transfer (FRET) is an important application that is currently under investigation in our laboratory. FRET can be measured by monitoring the decrease in lifetime of the donor fluorophore as it nonradiatively transfers energy to an acceptor that is typically within a distance of 10 nm. In applications where FRET occurs because of the formation of a protein complex, the spatial configuration of the donor and acceptor is fixed upon binding, which determines the decrease in the donor lifetime. Thus, when FRET is imaged with FLIM, the decay model may be assumed to be biexponential with spatially invariant lifetimes, and global analysis should provide a powerful tool for evaluating the populations and properties of bound and unbound protein states in cells.

PJV was supported by a long-term fellowship from the European Molecular Biology Organization (EMBO).

REFERENCES

Bastiaens, P. I. H., and T. M. Jovin. 1996. Microspectroscopic imaging tracks the intracellular processing of a signal transduction protein: fluorescent-labeled protein kinase C βI. *Proc. Natl. Acad. Sci. USA.* 93: 8407–8412.

Bastiaens, P. I. H., and A. Squire. 1999. Fluorescence lifetime imaging microscopy: spatial resolution of biochemical processes in the cell. *Trends Cell Biol.* 9:48–52.

Beechem, J. M. 1992. Global analysis of biochemical and biophysical data. *Methods Enzymol.* 210:37–54.

Beechem, J. M., M. Ameloot, and L. Brand. 1985. Global and target analysis of complex decay phenomena. *Anal. Instrum.* 14:379–402.

Beechem, J. M., and L. Brand. 1986. Global analysis of fluorescence decay: applications to some unusual experimental and theoretical studies. *Photochem. Photobiol.* 44:323–329.

Beechem, J. M., J. R. Knutson, J. B. A. Ross, B. W. Turner, and L. Brand. 1983. Global resolution of heterogeneous decay by phase/modulation fluorometry: mixtures and proteins. *Biochemistry.* 22:6054–6058.

Buurman, E. P., R. Sanders, A. Draaijer, H. C. Gerritsen, J. J. F. van Veen, P. M. Houpt, and Y. K. Levine. 1992. Fluorescence lifetime imaging using a confocal laser scanning microscope. *Scanning.* 14:155–159.

Carlsson, K., and A. Liljeborg. 1997. Confocal fluorescence microscopy using spectral and lifetime information to simultaneously record four fluorophores with high channel separation. *J. Microsc.* 185:37–46.

Clegg, R. M., B. A. Feddersen, A. E. Gratton, and T. M. Jovin. 1992. Time resolved imaging fluorescence microscopy. *Proc. SPIE.* 1640:448–460.

Clegg, R. M., and P. C. Schneider. 1996. Fluorescence lifetime-resolved imaging microscopy: a general description of lifetime-resolved imaging measurements. *In* Fluorescence Microscopy and Fluorescence Probes. J. Slavik, editor. Plenum Press, New York. 15–33.

Dong, C. Y., P. T. C. So, T. French, and E. Gratton. 1995. Fluorescence lifetime imaging by asynchronous pump-probe microscopy. *Biophys. J.* 69:2234–2242.

Draaijer, A., R. Sanders, and H. C. Gerritsen. 1995. Fluorescence lifetime imaging, a new tool in confocal microscopy. *In* Handbook of Biological Confocal Microscopy, 2nd Ed. J. B. Pawley, editor. Plenum Press, New York. 491–505.

French, T., P. T. C. So, D. J. Weaver, Jr., T. Coelho-Sampaio, E. Gratton, E. W. Voss, and J. Carrero. 1997. Two-photon fluorescence lifetime imaging microscopy of macrophage-mediated antigen processing. *J. Microsc.* 185:339–353.

Gadella, T. W. J., Jr., R. Clegg, and T. M. Jovin. 1994. Fluorescence lifetime imaging microscopy: pixel-by-pixel analysis of phase-modulation data. *Bioimaging.* 2:139–159.

Gadella, T. W. J., Jr., and T. M. Jovin. 1995. Oligomerization of epidermal growth factor receptors on A431 cells studied by time-resolved fluorescence imaging microscopy—a stereochemical model for tyrosine kinase receptor activation. *J. Cell Biol.* 129:1543–1558.

Gadella, T. W. J., Jr., T. M. Jovin, and R. M. Clegg. 1993. Fluorescence lifetime imaging microscopy (FLIM)—spatial resolution of microstructures on the nanosecond time-scale. *Biophys. Chem.* 48:221–239.

Gadella, T. W. J., Jr., G. N. M. van der Krogt, and T. Bisseling. 1999. GFP-based FRET microscopy in living plant cells. *Trends Plant Sci.* 4:287–291.

Golub, G. H., and V. Pereyra. 1973. The differentiation of pseudo-inverses and nonlinear least squares problems whose variables separate. *SIAM J. Numer. Anal.* 10:413–432.

Gratton, E., and M. Limkeman. 1983. A continuously variable frequency cross-correlation phase fluorometer with picosecond resolution. *Biophys. J.* 44:315–324.

Gratton, E., M. Limkeman, J. R. Lakowicz, B. P. Maliwal, H. Cherek, and G. Laczko. 1984. Resolution of mixtures of fluorophores using variable-frequency phase and modulation data. *Biophys. J.* 46:479–486.

Jovin, T. M., and D. J. Arndt-Jovin. 1989. FRET microscopy: digital imaging of fluorescence resonance energy transfer. *In* Cell Structure and Function by Microspectrofluometry. E. Kohen and J. G. Hirschberg, editors. Academic Press, San Diego. 99–115.

Knutson, J. R., J. M. Beechem, and L. Brand. 1983. Simultaneous analysis of multiple fluorescence decay curves: a global approach. *Chem. Phys. Lett.* 102:501–507.

Kume, H., K. Koyama, K. Nakatsugawa, S. Susuki, and D. Fatlowitz. 1988. Ultrafast microchannel plate photomultipliers. *Appl. Opt.* 27: 1170–1178.

Lakowicz, J. R., and K. Berndt. 1991. Lifetime-selective fluorescence imaging using an rf phase-sensitive camera. *Rev. Sci. Instrum.* 62: 1727–1734.

Lakowicz, J. R., G. Laczko, H. Cherek, E. Gratton, and M. Limkeman. 1984. Analysis of fluorescence decay kinetics from variable-frequency phase shift and modulation data. *Biophys. J.* 46:463–477.

Lakowicz, J. R., H. S. K. Nowaczyk, and M. L. Johnson. 1992. Fluorescence lifetime imaging of free and protein-bound NADH. *Proc. Natl. Acad. Sci. USA.* 89:1271–1275.

Lakowicz, J. R., H. Szmacinski, W. J. Lederer, M. S. Kirby, M. L. Johnson, and K. Nowaczyk. 1994. Fluorescence lifetime imaging of intracellular calcium in COS cells using Quin-2. *Cell Calcium.* 15:7–27.

Ng, T., A. Squire, G. Hansra, F. Bornancin, C. Prevostel, A. Hanby, W. Harris, D. Barnes, S. Schmidt, H. Mellor, P. I. H. Bastiaens, and P. J. Parker. 1999. Imaging protein kinase Cα activation in cells. *Science.* 283:2085–2089.

Pepperkok, R., A. Squire, S. Geley, and P. I. H. Bastiaens. 1999. Simultaneous detection of multiple green fluorescent proteins in live cells by fluorescence lifetime imaging microscopy. *Curr. Biol.* 9:269–272.

Periasamy, A., P. Wodnicki, X. F. Wang, S. Kwon, G. W. Gordon, and B. Herman. 1996. Time-resolved fluorescence lifetime imaging microscopy using a picosecond pulsed tunable dye-laser. *Rev. Sci. Instrum.* 67: 3722–3731.

Press, W. H., S. A. Teukolsky, and W. T. Vetterling. 1992. Numerical Recipes in C, 2nd Ed. Cambridge University Press, Cambridge.

Sanders, R., A. Draaijer, H. C. Gerritsen, P. M. Houpt, and Y. K. Levine. 1995. Quantitative pH imaging in cells using confocal fluorescence lifetime imaging microscopy. *Anal. Biochem.* 227:302–308.

Schlick, T., and A. Fogelson. 1992. TNPACK—a truncated Newton minimization package for large-scale problems. I. algorithm and usage. *ACM Trans. Math. Soft.* 18:46–70.

Schneider, P. C., and R. M. Clegg. 1997. Rapid acquisition, analysis, and display of fluorescence lifetime-resolved images for real-time applications. *Rev. Sci. Instrum.* 68:4107–4119.

Scully, A. D., A. J. MacRobert, S. Botchway, P. O'Neill, A. W. Parker, R. B. Ostler, and D. Phillips. 1996. Development of a laser-based fluorescence microscope with subnanosecond time resolution. *J. Fluoresc.* 6:119–125.

Scully, A. D., R. B. Ostler, D. Phillips, P. O. O'Neill, K. M. S. Townsend, A. W. Parker, and A. J. MacRoberts. 1997. Application of fluorescence lifetime imaging microscopy to the investigation of intracellular PDT mechanisms. *Bioimaging.* 5:49–63.

So, P. T. C., W. N. Yu, K. Berland, C. Y. Dong, and E. Gratton. 1995. Time-resolved fluorescence microscopy using two-photon excitation. *Bioimaging.* 3:1–15.

Squire, A., and P. I. H. Bastiaens. 1999. Three dimensional image restoration in fluorescence lifetime imaging microscopy. *J. Microsc.* 193: 36–49.

Squire, A., P. J. Verveer, and P. I. H. Bastiaens. 2000. Multiple frequency fluorescence lifetime imaging microscopy. *J. Microsc.* 197:136–149.

Sytsma, J., J. M. Vroom, C. J. de Grauw, and H. C. Gerritsen. 1998. Time-gated fluorescence lifetime imaging and microvolume spectroscopy using two-photon excitation. *J. Microsc.* 191:39–51.

Szmancinski, H., and J. R. Lakowicz. 1995. Possibility of simultaneously measuring low and high-calcium concentrations using Fura-2 and lifetime-based sensing. *Cell Calcium.* 18:64–75.